NON-NEWTONIAN FLUID ANALYTICAL FILLING TIME MODEL WITH CONTACT LINE JUMP UNDERFILL ENCAPSULATION

NG FEI CHONG

UNIVERSITI SAINS MALAYSIA

2019

NON-NEWTONIAN FLUID ANALYTICAL FILLING TIME MODEL WITH CONTACT LINE JUMP UNDERFILL ENCAPSULATION

By

NG FEI CHONG

Thesis submitted in fulfilement of the requirements for the degree of Doctor of Philosophy

June 2019

ACKNOWLEDGEMENT

My foremost gratitude is extended to all my family members, especially my parents and aunts, for their continuous support and understanding throughout my study.

I would like to express my warmest appreciation to my main supervisor, Dr. Aizat, whom gave me tremendous advices, guidance and helping hands throughout my research. Similarly goes to my co-supervisor, Prof. Zulkifly.

The assistances provided by Mr. Norijas, Dr. Ooi, Mr. Lim and Mr. Tan on the experiment are appreciated. I would like to thank Mr. Yusuf from Jabil Circuit Sdn. Bhd. on the technical advices and benchmarking data. The valuable discussions with Mr. Teoh, Mr. H'ng, Mr. Tung, Dr. Hafifi, Mr. Aqil, Mr. Leong and Ms. Tang were gratefully appreciated. The assistances given by Mdm. Asfarina was acknowledged. Not forgetting the generosity shown by Dr. Yu, Mr. Lee and Mr. H'ng. The list is extended to all my friends: Mr. Tan, Mr. Lee and Mr. Lim.

On the financial support, I would like to acknowledge the Universiti Sains Malaysia (USM) Fellowship award. Additionally, the research grants provided by Dr. Aizat also partly funded my research work on setup, computer, printer and papers.

I would like to thank the Thesis Examination Panel for giving me invaluable criticisms and constructive comments to improve the quality of thesis.

At this very point of writing, my postgraduate study concluded. It was a long journey filled with joy, gratitude and accomplishment coupled with hardship, dilemma and challenge. That to be said, it was not a smooth sailing. Still, I am fortunate to meet with helpful people whom aided me through this journey and eventually completed it, either directly or indirectly.

TABLE OF CONTENTS

	Page
ACKNOWLEDGEMENT	**ii**
TABLE OF CONTENTS	**iii**
LIST OF TABLES	**vi**
LIST OF FIGURES	**vii**
LIST OF SYMBOLS	**xii**
LIST OF ABBREVIATIONS	**xiv**
ABSTRAK	**xv**
ABSTRACT	**xvi**

CHAPTER 1: INTRODUCTION

1.1 Research backgrounds	1
1.1.1 Electronic packaging	1
1.1.2 Flip-chip technology	2
1.1.3 Underfill process	2
1.2 Problem statements	6
1.3 Research objectives	8
1.4 Research contributions	8
1.5 Research Scope	9
1.6 Thesis outline	9

Page

CHAPTER 2: LITERATURE REVIEW

2.1 Experimental studies on flip-chip underfill 10

2.2 Underfill experiments based on imitate flip-chip 13

2.3 Numerical studies on flip-chip underfill 16

2.4 Analytical studies on underfill flip-chip 19

2.5 Generic study on capillary flow 25

2.6 Summary 27

CHAPTER 3: METHODOLOGY

3.1 Analytical filling time model 29

3.1.1 Scopes and Features 29

3.1.2 Formulations of Couette flow 31

3.1.3 Formulation for bump-level analysis 36

3.1.4 Filling efficiency 47

3.1.5 Dimensionless unit 48

3.1.6 Limitations 50

3.2 Numerical simulation 52

3.3 Scaled-up imitated flip-chip experiment 58

CHAPTER 4: RESULTS AND DISCUSSION

4.1 Overview 61

4.2 Spatial analysis 63

4.2.1 Meniscus evolution 63

4.2.2 Effect of bump pitch on meniscus evolution 68

Page

4.2.3 Effect of bump contact angle on meniscus evolution 76

4.2.4 Contact line jump 79

4.2.5 Bump contributed capillary pressure 82

4.3 Temporal analysis 85

4.3.1 Validation with experiment by Lee et al. (2010) 85

4.3.2 Validation with the experiment by Nyugen et al. (1999) 95

4.3.3 Validation with the experiment by Wan et al. (2008) 99

4.3.4 Validation with current experiment of scaled-up imitate flip-chip 100

4.3.5 Validation with industrial benchmarking of package-on-package 109

4.4 Dimensionless analysis 114

4.4.1 Dimensionless variable analysis 114

4.4.2 Generalized dimensionless analysis 125

4.4.3 Threshold and critical bump pitch 129

4.4.4 Critical contact angle 131

CHAPTER 5: CONCLUSION AND FUTURE RECOMMENDATIONS

5.1 Conclusion 133

5.2 Recommendations for future research 136

REFERENCES 137

APPENDIX

Appendix A: Derivation of equation (3.28)

Appendix B: Derivations of equation (3.48) and equation (3.49)

LIST OF PUBLICATIONS

LIST OF TABLES

		Page
Table 3.1	Comparison of the present analytical filling time model with the past models.	30
Table 3.2	Mesh independent study for long array unit-cells simulation.	55
Table 3.3	Mesh independent study for scaled-up imitated flip-chip.	56
Table 3.4	Material properties of primary and secondary phases.	57
Table 4.1	Usage of research methodologies on analysis sub-sections.	62
Table 4.2	Comparison of the filling time from current analytical model with that from the experiment by Lee et al. (2010), current numerical simulation and past analytical models.	86
Table 4.3	The discrepancy of filling time of various analytical models and numerical results as compared to the experimental data by Lee et al. (2010).	86
Table 4.4	Allocation of individual filling times components and the corresponding percentages for the underfill flow in flip-chip of various pitches.	89
Table 4.5	Efficiencies of underfill fluid flow in the flip-chips.	94
Table 4.6	Comparison of analytical filling times with the experimental findings by Nyugen et al. (1999) for the underfill process using three different fluids.	95
Table 4.7	Comparison of analytical and experimental (Nyugen et al., 1999) filing times for the underfill flow in test chip *Q*.	98
Table 4.8	Dimensionless numbers in actual and scaled-up systems.	101
Table 4.9	Root mean squared deviations of numerical and analytical filling times for the corresponding underfill experiment of scaled-up imitated flip-chip.	105
Table 4.10	Chip dimensions at each layer of the PoP (Tura Ali, 2016).	109
Table 4.11	Comparisons of benchmark and analytical filling times for the underfill flow of 3-stacks and 4-stacks PoP devices.	112
Table 4.12	Order of magnitude of the change in T_f^* due to parameters variation from the corresponding lower limit to the upper limit.	124

LIST OF FIGURES

		Page
Figure 1.1	Three hierarchy levels of electronic packaging (Sun, 2004).	1
Figure 1.2	Comparison of wire bond and flip-chip packages (Wan et al., 2007a).	2
Figure 1.3	Flip-chip assembly with capillary underfill (Zhang and Wong, 2004).	4
Figure 1.4	Flip-chip assembly with no-flow underfill (Zhang and Wong, 2004).	4
Figure 1.5	Molded underfill setup for flip-chip (Zhang and Wong, 2004).	5
Figure 3.1	Side-view (x-z plane) of the underfill fluid flow into the chip-substrate assembly during the flip-chip encapsulation process.	31
Figure 3.2	The pressure distribution for the capillary Couette flow.	35
Figure 3.3	Definition and representation of geometrical parameters in (*a*) the flip-chip bump array and (*b*) a unit cell model, as seen from the top (x-y plane).	36
Figure 3.4	Segmentation of unit cell into three regions of different filling stages: (*a*) bump region; (*b*) exit CLJ region and (*c*) bump-less region.	38
Figure 3.5	Schematic computational route of the current filling time model of underfill fluid flow in flip-chip.	38
Figure 3.6	Transient evolution of flow meniscus upon interacting with bumps.	39
Figure 3.7	Analytical meniscus evolution during the exit contact line jump (CLJ) and equilibrium flow front after CLJ by the joining of two adjacent convex menisci.	44
Figure 3.8	Comparison of proposed analytical and experimental (Lee et al., 2010) equilibrium contact lines, with the straighten contact lines during menisci merging as observed from the experiment by Lee et al. (2010).	44
Figure 3.9	Qualitative comparison of the menisci shape obtained from numerical mesh models I – V of the triple unit-cells simulation.	54

		Page
Figure 3.10	Overview of the triple unit-cells mathematical model.	54
Figure 3.11	Overview of long array unit cells mathematical model.	55
Figure 3.12	Overview of scaled-up imitated flip-chip mathematical model.	57
Figure 3.13	The closed-up view of 6 × 6 scaled-up imitated flip-chip with various bump pitches, W = 3.2 mm, 4.0 mm and 4.8 mm used in the underfill experiment.	59
Figure 3.14	List of all materials and apparatus used in the current experiment.	60
Figure 3.15	Setup of the underfill experiment of scaled-up imitated flip-chip.	60
Figure 4.1	Illustration of the (*a*) side principle plane as seen from the top and (*b*) top principle plane as seen from the side, for defining the meniscus shape.	64
Figure 4.2	Illustration of flow menisci subtended by the (*a*) bump surface in top principle plane and (*b*) both chip and substrate surfaces at side principle plane.	64
Figure 4.3	Comparison of experimental (Lee et al., 2010), numerical simulated and analytical predicted flow menisci at various filling stages, for the spatial parameters of $\theta_b = 55°$, $W =$ 0.10 mm and $d = 0.05$ mm.	67
Figure 4.4	Meniscus evolution of underfill fluid at various filling stages in a unit cell of dimensions $W \times W$ for the flip-chips with various pitches, W based on the experiment specifications described by Lee et al. (2010).	69
Figure 4.5	Designation of measuring parameters ℓ and t on the numerical simulated meniscus for the computation of meniscus parameters ϕ, R and γ.	70
Figure 4.6	Plot of angle subtended by the meniscus arc, γ against angular displacement, φ for d = 0.05 mm and $\theta_b = 55°$, regardless of the bump pitch, W.	72
Figure 4.7	Plot of radius of meniscus arc, γ against angular displacement, φ for various bump pitches, W for d = 0.05 mm and $\theta_b =$ 55°.	72

		Page
Figure 4.8	Plots of (*a*) center-line flow front displacement, S, that relative to the bump entrance and (*b*) its non-dimensionalized counterpart, $S^* = S/W$ against the angular displacement, for various bump pitches, W with d = 0.05 mm and $\theta_b = 55°$.	74
Figure 4.9	Evolution of flow meniscus subtended by two adjacent cylindrical bumps of various pitch sizes, W from the angular displacement of $-90°$ to $90°$, as seen from the principal plane. The fluid's contact angle respect to the bump surface is 55° and the separation between each consecutive isolines is 15°.	75
Figure 4.10	Variation plots of meniscus shape parameters, (*a*) γ, (*b*) R and (*c*) S against ϕ for various bump contact angles with W = 0.10 mm and d = 0.05 mm.	77
Figure 4.11	Evolution of flow meniscus subtended by two adjacent cylindrical bumps with $d = 0.05$ mm and $W = 0.10$ mm but various contact angles relative to bump surface, θ_b, from the bump's angular displacement of $-90°$ to $90°$, as seen from the principal plane. The separation between each consecutive isolines is 15°.	78
Figure 4.12	The current proposed contact line jump (CLJ) criterions and the corresponding post-jump equilibrium meniscus at both (*a*) entrant and (*b*) exit.	79
Figure 4.13	Plot of the angular position of equilibrium meniscus after the attach jump (entrant CLJ) for various pitches and bump contact angles.	81
Figure 4.14	Plot of the dimensionless filling distance of the equilibrium meniscus after the detach jump (exit CLJ) for various pitches and bump contact angles, together with the segmentations due to geometrical limitation.	81
Figure 4.15	Plot of $P^*_{c,b}$ against ϕ for various θ_b at fixed $W^* = 2$.	84
Figure 4.16	Plot of $P^*_{c,b}$ against ϕ for various W^* at fixed $\theta_b = 0°$.	84
Figure 4.17	Plot of $P^*_{c,b}$ against ϕ for various W^* at fixed $\theta_b = 60°$.	84
Figure 4.18	Plot of the contributions of individual filling time components on the overall filling time on flip-chip with various bump pitches, W.	89
Figure 4.19	Plot of meniscus flow velocity at various filling displacement.	91

		Page
Figure 4.20	Plot of capillary pressure magnitude at various flow front location.	91
Figure 4.21	Comparative plot of numerical and analytical filling progressions for the underfill flow in flip-chips of different pitches as described by Lee et al. (2010).	92
Figure 4.22	Numerical flow progression of underfill fluid in the one-pitch width flip-chips of different bump pitches, based on the experiment by Lee et al. (2010).	93
Figure 4.23	Analytical and experimental (Wan et al, 2008) filling progressions.	99
Figure 4.24	Scaling effect on the filling progression of underfill flow.	103
Figure 4.25	Qualitative comparison of experimental and numerical simulated flow fronts of the underfill flow in scaled-up imitate flip-chip with various bump pitches: (*a*) $W = 3.2$ mm, (*b*) $W = 4.0$ mm and (*c*) $W = 4.8$ mm.	104
Figure 4.26	Comparative plots of analytical, numerical and experimental relative filling progression for the underfill flow in the three scaled-up flip-chips of various pitches: 3.2 mm (top); 4.0 mm (middle) and 4.8 mm (bottom).	106
Figure 4.27	Comparative plots of numerical and analytical filling times for the underfill flow in scaled-up flip-chips of variables pitches.	108
Figure 4.28	Comparative plots of numerical and analytical volume fraction filled with underfill fluid in scaled-up flip-chips of variables pitches.	108
Figure 4.29	Solder bump arrangement layout of PoP (Tura Ali, 2016).	110
Figure 4.30	3-stacks and 4-stacks PoP devices before and after underfill (Tura Ali, 2016).	110
Figure 4.31	The Nordon ASYMTEK dispensing jetting used to underfill the PoP device (Tura Ali, 2016).	110
Figure 4.32	Apparent filling cells and path (in grey) of the double inlets (L-type) dispensing on middle empty package.	111
Figure 4.33	Plot of T_{f}^* against $x_{\mathrm{f},d}^* = x_{\mathrm{f}}/d$ for variable $W^* = W/d$ at fixed $\theta = 0°$ (top), $\theta = 30°$ (middle) and $\theta = 60°$ (bottom).	115

		Page
Figure 4.34	Plot of T_f^* against $x_{f,W}^* = x_f/W$ for variable $W^* = W/d$ at fixed $\theta = 0°$ (top), $\theta = 30°$ (middle) and $\theta = 60°$ (bottom).	116
Figure 4.35	Summary plot of dimensionless filing time when the flow reached the end of 30th unit cells at various pitch, W^* and wetting conditions ($\theta = 0°$, $30°$, $60°$).	117
Figure 4.36	Plot of T_f^* against $x_f^* = x_f/W$ for variable $h^* = h/d$ at fixed $\theta = 0°$ (top) and $\theta = 60°$ (bottom).	119
Figure 4.37	Summary plot of dimensionless filing time when the flow reached the end of 30th unit cells at various gap height, h^* and wetting conditions ($\theta = 0°$, $60°$).	119
Figure 4.38	Plot of T_f^* against x_f^* for variables $c^* = c/d$ at fixed $\theta = 0°$ (top) and $\theta = 60°$ (bottom).	120
Figure 4.39	Plot of T_f^* against x_f^* for variable n at fixed $\theta = 0°$ (top) and $\theta = 60°$ (bottom).	121
Figure 4.40	Plot of T_f^* against x_f^* for variable θ_b at fixed $\theta_c = \theta_s = 0°$ (top) and $\theta_c = \theta_s = 60°$ (bottom).	122
Figure 4.41	Plot of T_f^* against x_f^* for variable $\theta = \theta_c = \theta_s = \theta_b$.	123
Figure 4.42	Dimensionless plot of filling time at the absolute filling distance of $x_{f,d}^* = c_d^* + 30W^*$ against bump pitch for various h^* and θ.	125
Figure 4.43	Plot of absolute filling time coefficient, Π_d for the Washburn flow approximation model at various pitch, gap height and contact angle.	128
Figure 4.44	Threshold pitch of bump array, W_{th}^* at different contact angle, θ and gap height, h^* as subjected to the pressure and geometrical limitations.	130
Figure 4.45	Critical contact angle at various gap height, h^* for three different contact angle consideration cases.	132

LIST OF SYMBOLS

Symbol	Physical meaning	Unit
(x, y, z)	Three-dimensional spatial coordinates	mm
(u, v, w)	Three-dimensional flow velocity	mm/s
g	Gravitational acceleration	mm/s^2
τ	Stress tensor	Pa
$\dot{\gamma}$	Shear rate	s^{-1}
μ	Dynamic viscosity	Pa-s
m	Flow consistency index	kg/m-s
n	Flow behavior index	-
σ	Surface tension	N-m
θ_c	Contact angle at chip surface	deg
θ_s	Contact angle at substrate surface	deg
θ_b	Contact angle at bump surface	deg
h	Gap height	mm
W	Bump pitch	mm
d	Bump diameter	mm
c	Chip edge pre-bump length	mm
ϕ	Generalized angular displacement as seen from bump	deg
ϕ_j	Angular position of equilibrium attach jump meniscus	deg
ϕ_c	Critical angular displacement of meniscus	deg
S_j^*	Dimensionless maximal center-line flow displacement	-
x_{f}	Center-line filling distance	mm
x_{f}'	Modified filling distance for L-type dispensing	mm

S	Filling displacement in unit cell/Residual filling length	mm
R	Curvature radius of meniscus arc	mm
γ	Subtended angle of meniscus arc	deg
k	Number of unit-cell(s) passed	-
T_{f}	Filling time	s
U	Meniscus flow velocity	mm/s
Δp_c	Capillary pressure	Pa
f_n	Volume fraction filled of n-th fluid in multiphase system	-
F	Scaling factor of scaled-up imitated underfill system	-
η	Effective filling efficiency	-
η_t	Temporal filling efficiency	-
η_s	Spatial filling efficiency	-
W^*	Dimensionless bump pitch	-
h^*	Dimensionless gap height	-
c^*	Dimensionless chip edge length	-
θ	Equip contact angle	deg
T_{f}^*	Dimensionless filling time	-
$x_{\mathrm{f},d}^*$	Dimensionless absolute filling distance	-
$x_{\mathrm{f},d}^*$	Dimensionless relative filling distance	-
Π_d	Dimensionless absolute filling time coefficient	-
Π_W	Dimensionless relative filling time coefficient	-
W_{th}^*	Dimensionless bump pitch threshold	-
W_{c}^*	Dimensionless critical bump pitch	-
$\theta_{b,\mathrm{cr}}$	Critical bump contact angle	deg
θ_{cr}	Critical equip contact angle	deg

LIST OF ABBREVIATIONS

BGA	Ball grid array
CAD	Computer aided design
CLJ	Contact line jump
CTE	Coefficient of thermal expansion
FEM	Finite element method
FSI	Fluid/structure interaction
FVM	Finite volume method
I/O	Input/output
LBM	Lattice Boltzmann method
MpCCI	Mesh-based parallel code coupling interface
PCB	Printed circuit board
PG	Petrov-Galerkin
PIV	Particle image velocimetry
VOF	Volume of fluid
UV	Ultraviolet
μPIV	Micro particle image velocimetry

MODEL MASA PENGISIAN ANALITIK BENDALIR BUKAN NEWTONIAN DENGAN LONCATAN MENISKUS PENGKAPSULAN ISIAN BAWAH

ABSTRAK

Bilangan model masa pengisian untuk peramalan aliran kapilari bendalir isian bawah dalam flip-chip adalah terhad; manakala kejituan model-model yang sedia ada masih menpunyai ruang penambahbaikan ekoran daripada andaian media berpori. Lebihan lagi, sifat bukan Newtonian bendalir isian bawah tidak kerap dimodelkan. Lantaran itu, kajian ini menunjukkan sebuah model analitik baharu yang berasaskan analisi peringkat benjolan khas untuk bendalir isian bawah bukan Newtonian. Dengan kaedah pembahagian rantau, masa-masa pengisian dihitung secara berasingan di setiap peringkat pengisian. Model ini juga mengandungi formulasi spatial, yakni evolusi menikus dan loncatan meniskus yang telah dipertambahbaikan dan sejajar dengan hasil dapatan ujikaji dan simulasi. Seterusnya, tiga buah ujikaji isi bawah lepas dirujuk untuk mengesahkan kejituan model analitikal ini, bersama-sama dengan ujikaji berskala besar semasa dan penandaarasan industri. Secara keseluruhannya, model ini dapat meramalkan masa pengisian dengan kadar percanggahan yang paling rendah antara semua model analitik lepas bagi kesemua kes-kes pengesahan. Ini mengesahkan keupayaan model ini dari segi ketepatan dan fleksibiliti. Dua buah analisis temporal baru, iaitu komponen masa pengisian individu dan kecekapan pengisian diperkenalkan untuk menyelidik kesan pitch jajaran benjoran. Kemudian, model analitik ini digunakan untuk mengaji variasi parameter isi bawah terhadap perkembagan pengisian. Parameter yang paling mempengaruhi aliran isi bawah ialah ketinggian jurang, sudut sesentuh dan pitch jajaran. Akhir sekali, sebuah carta masa pengisian umum yang mengaitkan pekali masa pengisian kepada tiga parameter isi bawah telah dijanakan dengan model ini, supaya masa pengisian dapat dicari secara lansung.

NON-NEWTONIAN FLUID ANALYTICAL FILLING TIME MODEL WITH CONTACT LINE JUMP UNDERFILL ENCAPSULATION

ABSTRACT

The analytical filling time models to predict the capillary underfill flow in flip-chip are limited in amount; while the accuracy of existing models still has room of improvement due to the conventional porous media assumption. Moreover, the non-Newtonian behavior of underfill fluid was scarcely modelled. Therefore, this research presents a new filling time model based on novel bump-level analysis for the non-Newtonian power-law underfill fluid. Through the regional segregation approach, the filling times were separately studied at each filling stages. The formulation of current model had also incorporated both the spatial considerations of meniscus evolution and contact line jump, that were improvised in formulation and in-line to the experimental and numerical observations. Subsequently, three past underfill experiments were referred to validate with the current developed filling time model on top of the current scaled-up imitated flip-chip experiment and industrial package-on-package benchmarking. Overall, the current model predicted the filling times of least discrepancy among other existing analytical models for all validation cases. This had affirmed the capability of current model in terms of accuracy and versatility. Moreover, two new temporal analyses of individual filling time component and filling efficiency are introduced to further investigate the impact of bump pitch. Later, the well-validated analytical model is used to study the individual variation of underfill parameters on the filling progression. The parameters that affect the underfill flow prominently are gap height, contact angle and bump pitch. Lastly, a generalized filling time chart was generated using the current model to ease the direct computation of filling time.

CHAPTER 1

INTRODUCTION

1.1 Research backgrounds

1.1.1 Electronic packaging

Electronic packaging is the production of interconnection, enclosure and protection that bridging the silicon chip to become the final electronic products. Apart from completing the electronic circuits, the electronics packaging also provides heat dissipation mechanism, mechanical supports and protective layer against external environment. The electronic packaging aims to promote the reliability, productivity and longevity of the electronic device (Tummala et al., 1997; Sun, 2006).

Generally, there are three hierarchy levels of electronic package as shown in Figure 1.1. The first level being the interconnection between silicon die and module substrate, for instance wire bonding and flip-chip technology. Next, the second level represents the interconnection between the previous module substrate to the printed circuit board. In the third level packaging, the second-level packages were placed into a motherboard to complete the functionality of electronic device (Lau, 1994).

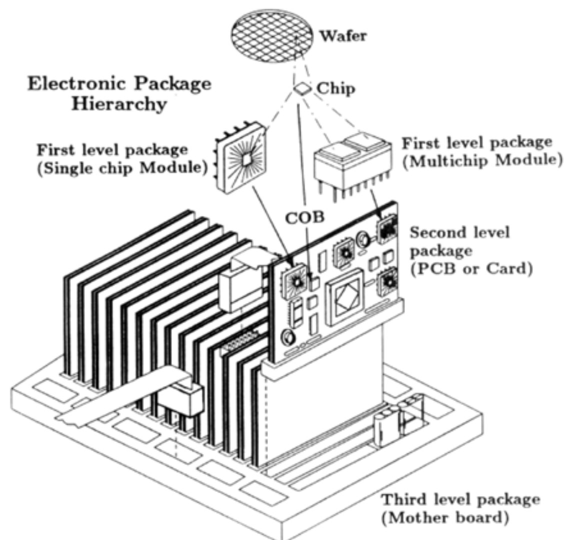

Figure 1.1 Three hierarchy levels of electronic packaging (Sun, 2004).

1.1.2 Flip-chip technology

With the increasing demands of electronics device of higher productivity and reliability but smaller and compact size, the flip-chip technology is introduced by connecting the active side of the silicon die to the substrate via the conducting bumps. In flip-chip, the active side of silicon die is flipped such that it faced the substrate; while in conventional wire bond package, the active side is always facing upward while the wires were drawn to connect the active side to the substrate, as illustrated Figure 1.2. In fact, it is justified that the flip-chip package is more advantageous than the conventional wire bond package in all aspects of input/output (I/O) density, electrical performance, size, production cost and thermal performance. Issue arises upon reducing the size of wire bond package while increasing its I/O count, where closer bonding wires will produce electromagnetic interference. Moreover, the peripheral side of the wires bonded to the substrate are getting shorter, thereby making the bonding process difficult and incurring additional costs (Wan et al., 2007a).

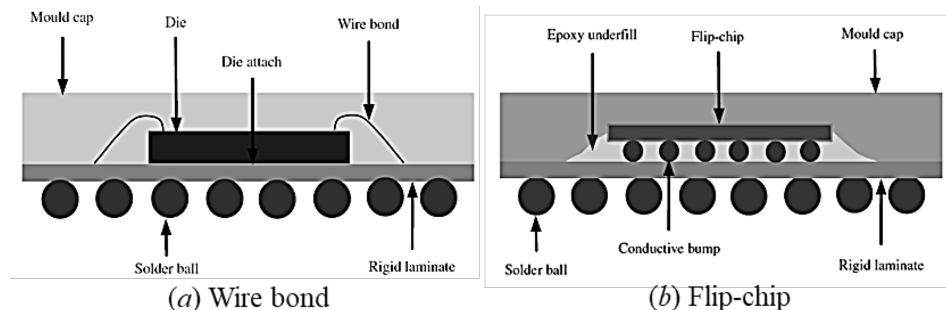

Figure 1.2 Comparison of wire bond and flip-chip packages (Wan et al., 2007a).

1.1.3 Underfill process

The major challenge posed by flip-chip packaging process is the thermal-mechanical stress due to the mismatch in the coefficient of thermal expansion (CTE) between the solder bump, the silicon chip and the organic substrate. As the usage of electronic device persists, the interconnectors of chip package are subjected to thermal

cycling and would result in fatigue or electrical failure (Ardebili and Pecht, 2009). The CTE mismatch issue can be addressed by filling the gap between the chip and substrate with appropriate material that will redistribute the thermal-mechanical stress away from the interconnector, for which such process is known as underfill (Tong, 2011). Usually, the underfill fluid that being dispensed into the gap is epoxy resin with filled fused silica. Upon cured under elevated temperature or presence of ultraviolet (UV) light, the underfill fluid that filled the gap between the bump array will chemically harden to form a protective layer that encapsulates the bumps. Despite the current described underfill process is conducted at the first level packaging of flip-chip, it is still being carried out at the second level packaging between the IC package and printed circuit board (PCB), such as ball grid array (BGA).

Generally, there are three variants of flip-chip underfill process: namely capillary, no-flow and molded. For the capillary underfill, the underfill fluid is gradually dispensed along one or more sides of the chip. Through the capillary action, the underfill fluid gradually flows into the gap between the chip and the substrate. This capillary underfill is regarded as the conventional underfill process that is able produce a complete flow with less probability of void formation. However, the capillary underfill flow is slow and requires substantially long filling time, as compared to the no-flow and molded underfill (Gordon et al., 1999).

Figure 1.3 summarized the process flow on the assembly, capillary underfill and curing of a flip-chip, during the first level packaging. After the flux is dispensed on the substrate board, the chip is aligned such that the attached bumps are vertically above the bond pad and being placed onto. Both the chip and substrate were heated in solder reflow to bond the solder bumps on the pads. Later, the flux dispensed earlier is cleaned using solver spray. Subsequently, the reliability of flip-chip is enhanced

through the implementation of capillary underfill process, where the underfill fluid is gradually dispensed along the peripheral side of chip. When the underfill fluid fully filled up the gap beneath, the flip-chip is sent to reflow for curing of underfill fluid.

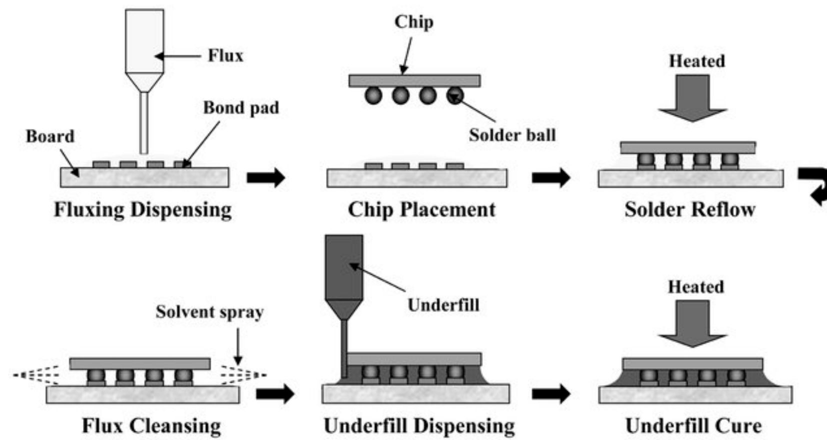

Figure 1.3 Flip-chip assembly with capillary underfill (Zhang and Wong, 2004).

In contrast, the no-flow underfill process is conducted by pre-dispensing certain amount of underfill fluid on the unmounted substrate. Then, the chip with solder bumps attached onto is aligned above the solder pad and being put on the substrate with underfill fluid. The placement of flip-chip on the substrate will result in the redistribution of underfill fluid such that it spreads horizontally to fill up the gap. Finally, the flip-chip assembly with underfill fluid are sent for reflow, to attach the bump on the solder pad as well as to cure the underfill fluid. The overall process flow of no-flow underfill is outlined in Figure 1.4. However, the air void is prone to formed in the no-flow underfill package due to the compression flow is difficult to control.

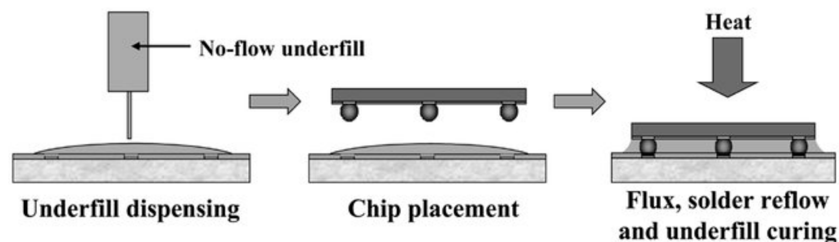

Figure 1.4 Flip-chip assembly with no-flow underfill (Zhang and Wong, 2004).

Molded underfill is an encapsulation process that utilizes injection or pressurize setup to attain a fast flow of underfill fluid. It is regarded as a solution to the slow underfill flow in conventional capillary underfill process, by applying external driving force. In Figure 1.5, the flip-chip is surrounded by a housing. Later, a stream of underfill fluid is injected through the mold inlet to fill up all the cavity in the flip-chip's housing. The molded underfill has some downsides where the defects of incomplete filling (Chai et al., 2002) and void formation due to air entrapment (Wan et al., 2007a; Ishak et al., 2016) are observed, thus affecting the package reliability.

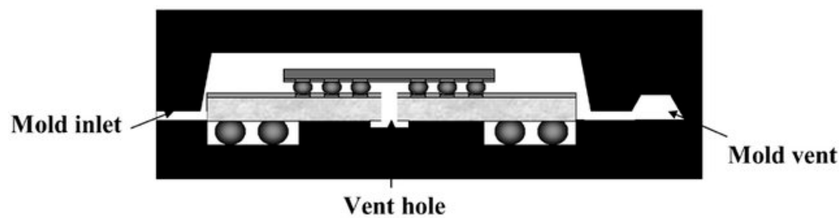

Figure 1.5 Molded underfill setup for flip-chip (Zhang and Wong, 2004).

In the industry, the underfill process is widely used in, but not limited to the microelectronics products for telecommunications, consumer electronics, life sciences and military. The selectively application of underfill process is largely due to the high materials and process costs, as well as its longer lead time. Accordingly, various researches have been conducted to optimize the process and to eliminate the defects, as a joint improvement to improve the process productivity and package reliability.

1.2 Problem statements

In the electronic packaging process, the filling time of the underfill flow is of utmost concern. Technically, long filling time will cause the occurrence of filler settling and incomplete filling, which later leads to void formation. Moreover, long lead time is generally not favored as it incurs additional manufacturing cost to the electronic assembly and later increases the selling price of the end-product. It can be seen that the original intention of underfill process to enhance the package reliability can be backfired. Therefore, various studies were conducted to improve the filling time by altering the flip-chip design and material composition of the underfill fluid.

The researches on underfill flow and filling time were mainly conducted by means of experiment and numerical simulation. However, the costly industrial standard underfill fluid and flip-chips as used in experiment are lack of controllable variations since these were readily manufactured by the supplier. While the downsides of experiment were able be addressed by the numerical simulations, there rise other issues revolving around the long computational time and simplification made on the numerical model. Furthermore, another flaw exists in conventional experiment is that the flip-chips are opaque, so the flow front during underfill cannot be visualized. To address this particular flaw, another variant of experiment is conducted by using similar imitated chip which is made of inexpensive transparent materials, for instance glass (Lee et al., 2010; Kim et al., 2011) and scaled-up Perspex (Khor et al., 2012; Abas et al., 2016). While the latter scaled-up approach is adopted to further enhance the flow visualization, additional justification on its scaling validity is required.

Alternatively, the underfill flow can be studied analytically based on the physics of capillary flow by deriving the filling time model. Unfortunately, such analytical works are scarce, mainly due to difficulty in the formulation and

mathematical framework. The formulation can be eased by making reasonable assumptions but at the cost of omitting certain flow details and ultimately the accuracy is at stake. Some of the assumptions made in the past analytical models are unnecessary while few being not aligned to the experimental and numerical observations.

Most of the previous analytical models rely on Darcy's law using porous media assumption, such that the filling time prediction is based on chip-level. Consequently, the exact mechanism of underfill flow in bump array were not detailed. For instance, the contact line jump (CLJ) phenomenon as discovered by Young (2003) was not well established in the analytical work nor being thoroughly investigated. This will affect the accuracy of predicted filling time.

With the escalating demands on miniature electronics devices and high-performance multi-layers stacking packages, the underfill process possess an even greater challenge. Eventually various studies on underfill parameters variation is conducted to optimize the underfill process. Versatility is the main criteria sought-after in both the variation and optimization studies of underfill process. Experimental variable studies are not viable due to the high incur costs and lack of customizable flip-chip and underfill fluid. Henceforth, numerical simulation will serve as a substitute, but suffers from long computational time. Meanwhile, the available filling time models are not qualitatively sufficient for the optimization study due to oversimplification.

Moreover, there is no comprehensive study that gives the filing time for any pairs of underfill fluids and flip-chips. This is also known as the generalized study and equivalent to the Moody diagram and psychrometric chart. In this generalized study, all the findings of parameters variation study will be integrated into a single chart to be applied for all underfill system. Through this generalized chart, the filling time for underfill system for wide ranges of underfill parameters can be determined directly.

1.3 Research objectives

(*a*) To develop a new bump-level analysis based analytical filling time model that generalized the non-Newtonian capillary flow in cylindrical bump array, for the prediction of underfill flow in flip-chip.

(*b*) To study the meniscus evolution of underfill flow analytically and thus improve the equilibrium criterions for both entrance and exit contact line jumps (CLJ).

(*c*) To validate the current developed analytical filling time model using findings from the current FVM numerical simulation and scaled-up experiment, as well as the experimental data and analytical filling time models from past literatures;

(*d*) To generalize the individual contribution of each underfill parameters on the filling progression, through non-dimensionalization.

1.4 Research contributions

(*a*) The development of a new bump-level analysis based analytical filling time model for the prediction of non-Newtonian capillary flow in bump array for the application of flip-chip underfill process, which was proven by its veracity and versatility upon been compared to the current and past experimental data, as well as the past analytical models.

(*b*) A thorough analytical study on the meniscus evolution, including the improvement of both entrance and exit contact line jumps of underfill flow.

(*c*) The introduction of two new temporal analyses for the underfill flow process, for instance the individual filling time component and the filling efficiency.

(*d*) The construction of a generalized dimensionless filling time chart at various underfill parameters together with the introduction of critical bump pitch and critical contact angle for the future optimization works.

1.5 Research Scope

This research primarily focuses on the development of new analytical filling time model to predict non-Newtonian capillary underfill flow in flip-chip and its meniscus evolution. As the current model is designed for capillary underfill flow, there exists a lower pitch threshold of investigated flip-chip for allowable underfill flow. Subsequently, finite volume method (FVM) based numerical simulations and underfill experiment using scaled-up imitated flip-chips are conducted to validate the new established analytical filling time model. The experimental data and analytical models from the past literatures together with the industrial benchmark time are used to additionally affirm the veracity of current analytical model. Subsequently, the well-validated analytical model is used to investigate the effect of parameters variation on the filling progression by means of non-dimensionalization. Finally, a generalized filling time chart is generated analytically to ease the determination of filling time in the underfill system of wide range of parameters.

1.6 Thesis outline

This thesis consists of five chapters. The first chapter introduces the research background of flip-chip underfill, problem statements, research objectives, research contributions and research scopes. Next, Chapter 2 presents the literatures reviews on flip-chip underfill and analytical filling time model. Chapter 3 details the methodology of analytical filling time model, numerical simulation and physical experiment. The studies of meniscus evolution and contact line jump, validation of current analytical filling time, dimensionless parameters variation and generalized filling time chart are then presented and discussed in Chapter 4. Lastly, this thesis is concluded in Chapter 5 together with the recommendation for future works.

CHAPTER 2

LITERATURE REVIEW

2.1 Experimental studies on flip-chip underfill

Physical experiment is the main approach to directly study the flip-chip underfill process. As both actual flip-chip and underfill fluid of industrial standard were used, it is regarded as the most accurate and realistic research methodology without much assumptions made. There are few underfill experimental works that highly acknowledged by the subsequent researchers in related fields, particularly Han and Wang (1997a), Nyugen et al. (1999) and Wan et al. (2008).

Han and Wang (1997a) performed experiment on the dispensing underfill process of IBM flip-chip. They additionally analyzed the material properties of the underfill fluid used, by obtaining the correlations of viscosity with curing kinetics, shear rate and temperatures. To verify the experimental results, the underfill flow fronts were simulated numerically based on Hele-Shaw approximation and modified analytical model by Washburn (1921). It is shown that the consideration of dynamic contact angle is able to give close prediction of numerical and analytical filling times with respect to the experimental time. Later, they also conducted another experiment on pressurized underfill of flip-chip (Han and Wang, 1997b), where the filling time is drastically reduced up to a factor of 1000 compared to the capillary underfill.

Nyugen et al. (1999) also conducted a series of flip-up underfill experiments using three distinct non-Newtonian underfill fluids. The variation of underfill fluid viscosity with shear rate were experimentally measured and later being fitted into the power-law constitutive equation by Wan et al. (2005a). The most prominent finding reported is the racing effect, where the edge flow being faster than the center flow, and may results in void formation. The experimental findings were validated using PLICE-

CAD flow simulation, but both the simulated and experimental flow front are not comparable due to the absence of racing effect in the former flow front.

The underfill experiments on two parallel plates with variables gap height and 6 mm × 6 mm flip-chip using non-Newtonian underfill fluid is carried out by Wan et al. (2008). The viscosity of the underfill fluid is based on power-law in which its coefficients were determined experimentally. For validation works, the analytical models by Washburn (1921) and Wan et al. (2005a) were used. It is reported that the latter gives much closer prediction of filling time upon compared to experimental findings, because of Washburn model did not incorporated the bump effect.

Peng and Young (2010) experimentally investigated the underfill flow in flip-chips of different bump pitches ranging from 225 – 325 μm and were numerically validated, using the finite element code by Young and Yang (2002b). Both the experimental and numerical filling times found to be comparable. It is reported that larger bump pitch gives higher filling rate, thus a faster completion of underfill process.

Another capillary underfill process of flip-chip package study is conducted by Lee et al. (2011). Two different non-Newtonian underfill encapsulants are dispensed on each of the two distinct flip-chips. The underfill process is later numerically simulated using ANSYS Fluent software for validation. The filling progressions achieved great consensus for all experiment, simulation and analytical Wan model.

Gwon et al. (2014) studied the effect of injection types (I, L and U) on the underfill flow in flip-chip packaging. The I, L and U injections respectively correspond to single, double and triple peripheral dispensing inlets. The underfill process was then numerically simulated using ANSYS Fluent software to affirm the experimental findings. They demonstrated that U-type gives faster completion rate, followed by L-type and finally I-type; but U-type injection can potentially leading to void formation.

Guo and Young (2015) also performed experiment on molded underfill process to investigate the vacuum effect on the void formation. They concluded that the lower the packaging pressure, the smaller air packet (void) is observed.

Experiments were conducted to study the material aspects of underfill fluid, for instance viscosity and contact angle. Typically, the underfill fluid consists of epoxy resin monomer, fused silica (SiO_2) filler and curing agent. The viscosity of the underfill fluid is largely dependent on the amount of SiO_2 added, such that the more filler content, the higher the viscosity (Sun, 2006; Tong, 2011).

The rheological properties of underfill fluid, for instance contact angle, surface tension and viscosity were experimentally measured by Wang (2002). The viscosity of underfill fluid is dependent on both the temperature and time (i.e. shear rate); whereas for the contact angle and viscosity are only dependent on the temperature.

In the experimental study by Sun et al. (2005), the viscosity of nanosilica composite underfill fluid is reduced through the silica surface modification using epoxy silane. This would greatly enhance its flowability during the underfill process and thus the filling time.

Wang (2007) experimentally determined the underfill fluid's viscosity. Also, by using the scanning electron microscope, the cross-sectional cut of a cured flip-chip underfill was inspected for void and filler settling. It is found that at low filler loading, the underfill fluid exhibits Newtonian fluid property. At short filling time, the filler settling is reduced. Moreover, underfill fluid of low viscosity favors the void formation.

Shan and Chen (2018) developed a new viscosity model for the encapsulant that incorporated the factors of shear rate, temperature and curing. The encapsulant's viscosity is experimentally measured at various temperatures and shear rates, which later were fitted into the Bird-Carreau model with Arrhenius equation.

2.2 Underfill experiments based on imitated flip-chip

While all the previously discussed experimental works relied on actual flip-chip, there are also literatures that perform underfill experiments using imitated flip-chip of actual scale or even scaled-up. Usually, the chip is replaced with a clear transparent material of similar wettability. The purposes of adopting imitated flip-chip is to enhance the visualization aspect as well as the versatility of parameters variation.

Wang (2005) used a pair of microscope glass slides to determine the filling time of various underfill fluids. The experimental time is in good agreement with the analytical prediction by Washburn (1921). It was reported that the fluid's viscosity played a major role in determining the filling time.

Silicon on glass flip-chips of variables pitches of 80 μm, 100 μm, 120 μm and 160 μm were fabricated by Lee et al. (2010) and Kim et al. (2011) for their works. The underfill fluid used in the experiment is replaced with glycerin that possess similar material properties as conventional industrial underfill fluid. Through micro particle image velocimetry (μPIV), the underfill fluid flow across the bump array were visualized and the fluid velocity contours were obtained. In the validation work, the analytical filling times predicted by Wan model are the closest to experimental times, but unable to compute the time for 80 μm pitch case. A handful of impactful findings were reported, for instance the occurrence of contact line jump in both bump entrance and exit were observed experimentally for the first time. Moreover, the variation of flow front velocity along the wetting distance is first-ever reported. Furthermore, the filling time at a given distance decrease with the increase in bump pitch, similar to the finding reported by Peng and Young (2010). The glass flip-chip system was also used by Shih and Young (2010) where both the chip and substrate were made from glass for observing the underfill flow front. Six underfill cases of flip-chip with varying

pitches from 200 μm to 325 μm were studied. It was found that the variation of bump pitches does not change the filling time much. Besides, the edge channel flow can be eliminated with full array flip-chip.

Another variant of underfill experiment that is based on homogenously scaled-up imitated chip to study the molded underfill encapsulation process. In the experimental setup described by Khor et al. (2012a), two sets of imitated chips were constructed using imitated bumps of different heights 0.40 cm and 0.65 cm. During the experiment, the underfill fluid stored inside a steel container was injected into the imitated chip via an injection plunger which controlled by a computer. It was found that air void formation be reduced by increasing the packaging pressure. Similar scaled-up chip setup was used again by Khor et al. (2012b) to study the effect of stacking chips and inlet positions on void formation, which concluded that the unstable flow front caused the void formation. The stacked imitated chips that consists of two layers was constructed by Ong et al. (2012). This setup of imitated chip and mold injection was also used by Khor et al. (2012c) to visualize the chip deformation during the molded encapsulation process and later compared to the numerical findings. Again, the scaled-up imitated chip was used by Khor and Abdullah (2013) to study the fluid/structure interaction of molded underfill process upon varying the thickness of imitated chip. Lastly, the study of effect of bump arrangement on molded encapsulation by Khor et al. (2014) also utilized the scaled-up imitated chip as the validation tool to their numerical models. Overall, despite all experiment findings were numerically validated, the vital scaling validity in terms of dynamic similarity and homogeneity were not discussed.

The idea of scaled-up imitated chip is extended for the studies of underfill process of ball grid array (BGA) device. BGA is the second level packaging, which

serves as the housing of flip-chip, that is attached to the PCB or motherboard. As a result, the overall dimensions of BGA is slightly larger than that of flip-chip. The first BGA underfill research with such setup was conducted by Abas et al. (2016a), to study how BGA bump arrangements (perimeter, middle empty and full array) affects the filling time. The underfill flow in perimeter registered the shortest filling time; while the full array has longest filling time. Abas et al. (2016b) used scaled-up BGA to comprehensively investigate the variation effects of the dispensing conditions (I-type, L-type and U-type) together with bump arrangements on the underfill process. Furthermore, the underfill flow fronts attained from BGA of different scale sizes were compared to justify the qualitative invariance of underfill flow front to scaling. The void formation is also investigated based on the factors of scale size, dispensing condition and bump arrangement (Abas et al., 2018). Apart from the observation of void in U-type dispensing, the larger scale-size of BGA also gave air void of larger size.

2.3 Numerical studies on flip-chip underfill

Generally, the flip-chip underfill process is numerically simulated to validate the experimental findings. Otherwise, new numerical scheme was proposed to simulate the underfill process, and being validated based on existing underfill experiments.

Hang and Wang (1997a) simulated the flow front through the Hele-Shaw approximation while considering the curing kinetics in underfill fluid. Nyugen et al. (1999) also numerically investigated the flip-chip underfill process using PLICE-CAD software. Nonetheless, the racing effect was not successfully being simulated. For the molded encapsulation of TQFP package, Nyugen et al. (2000) used the previous simulation software to visualize the underfill flow profiles. Kulkarmi et al. (2004) on other hand used characteristic based split Finite Element Method (FEM) to study the two-dimensional flow simulation for underfill process. Additionally, Lai et al. (2004) and Shen et al. (2006) simulated the underfill flow using the control volume FEM. Subsequently, Hashimotoa et al. (2008) presented the artificial compressibility method to numerically simulate the three-dimensional capillary and no-flow underfill flows.

Apart from FEM, the finite volume method (FVM) numerical scheme was used in underfill simulation. Wan et al. (2009) used FVM based numerical simulation, ANSYS Fluent to simulate their underfill experiment as reported in Wan et al. (2008), where both the experimental and numerical flow front and filling time are comparable. Besides, the pressurized flip-chip underfill process (Khor et al., 2010a) and capillary flip-chip underfill process (Khor et al., 2012d) were numerically simulated using FVM software, Fluent. Moreover, by using similar FVM software, the effect of bump arrangement on underfill fluid was numerically studied in Khor et al. (2010b), Ong et al. (2012) and Abas et al. (2016b). Meanwhile, Ong et al. (2013) numerically demonstrated the effect of microbump pitch of molded underfill process.

Another numerical method that was substantially used in researching the underfill process was the fluid/structure interaction (FSI), that is based on FVM discretization (Khor et al., 2011a). It is particularly useful to study the molded or injection underfill encapsulation, where the pressure exerted on the underfill fluid during injection will be imparted to the solder bumps and chip. On the contrary, the driving capillary force in conventional underfill process is relatively small in magnitude, thus the structural deformation of bump and chip due to the capillary flow is negligible. The simulation software involved in FSI were FLUENT and ABAQUS which is coupled by the mesh-based parallel code coupling interface (MpCCI). Various parameter variation studies for molded underfill process were conducted, for instance, inlet gates and gap height (Khor et al., 2011a), inlet pressure (Khor et al., 2011b), inlet position (Khor et al., 2012b) and bump shape (Khor et al., 2012e). Using the response surface methodology, optimization work on FSI aspect of molded underfill was performed by Khor et al. (2012e). Continuing the legacy of Khor's works on FSI, few additional follow-up studies on moulded underfill process were conducted based on the parameter variation of the aspect ratio (Ishak et al., 2015; Ishak et al., 2017a) and the stacking layout (Ishak et al., 2017b).

Wang et al. (2011) introduced new numerical scheme for the simulation of underfill flow in flip-chip. The governed equations were solved by the Petrov-Galerkin (PG) methods, while the PLIC-FAN method was used to track the flow front.

Abas et al. (2015) used the lattice Boltzmann method (LBM) numerical scheme to simulate the underfill process in BGA. The LBM simulated underfill flow front is compared to that attained from FVM simulation, while bubbles formation can be observed in the case of LBM. Later, Abas et al. (2016a) numerically studied the effect of bump arrangement on underfill flow in BGA, using LBM. Ishak et al. (2016) used

LBM for the simulation of molded underfill process, for which the micro-void formation was successfully observed.

Wang et al. (2016) also adopted the LBM to simulate the underfill flow fronts based on the past underfill experiment (Han and Wang, 1997a). The experimental and simulated flow fronts were found to be qualitatively comparable. However, the quantitative validation (i.e. filling time, velocity, pressure) was not presented.

Zhu et al. (2018) proposed a new dynamic pressure boundary condition for flip-chip underfill simulation and successfully predicted the racing effect as reported in the previous experimental work by Nyugen et al (1999).

The level-set method used in the numerical work by Wang et al. (2018) instead of conventional volume of fluid (VOF) method to capture the flow front of underfill fluid, for which it was well-validated with the experimental filling times for the underfill flow reported in Nyugen et al. (1999) and Lee et al. (2010).

2.4 Analytical studies on underfill flip-chip

Generally, the analytical underfill works aim to obtain the filling time elapsed of the underfill flow at different filling distance, in terms of length dimensions of the bump array and material properties of the underfill fluid. This is known as the filling time model. Nonetheless, the literatures on analytical study of flip-chip underfill were scarce in amount. This is caused by the complexity in derivation, so the more straightforward experiment and simulation methodologies were opted instead. Due to the lack of modelling and innovation approaches together with accuracy concern, there are only six distinct filling time models that were developed to date.

Dated back to about a century ago, Washburn (1921) derived the first equation that gives the relationship between the flow time, t_{f} and flow distance, x_{f} for the capillary flow in horizontal gap between two parallel plates, written as:

$$t_{\mathrm{f}} = \frac{3\mu x_{\mathrm{f}}^2}{\sigma h \cos\theta}, \tag{2.1}$$

where μ is the dynamic viscosity, σ is the surface tension, h is the gap height and θ is the contact angle at the plate surface. This corresponds to the capillary flow in viscous regime where the inertia effect diminished, gives the Washburn's relation of $t \sim x^2$.

The application of Washburn model on flip-chip underfill study is embarked by Han and Wang (1997a). The authors modified the Washburn model by considering the dynamic contact angle using the correlation equation by Newman (1968):

$$t_{\mathrm{f}} = \frac{3\mu x^2}{\sigma h \cos\theta_e} + \frac{a}{c}\left(1 - e^{-ct_{\mathrm{f}}}\right), \tag{2.2}$$

where θ_e is the equilibrium contact angle with both a and c being constants depending on the surface. The filling time, t_{f} is then solved iteratively. However, as the Washburn model did not incorporate the bump array, the filling time of the capillary underfill process will be greatly underestimated by a discrepancy up to 70% (Yao et al, 2014b).

In fact, the consideration of bump in analytical filling time model is pioneered by Young's research group. Young and Yang (2002a, 2002b) formulated the variable capillary pressure difference of meniscus due to varying gap and orientation between two adjacent bumps of pitch W, as a function of bump angular displacement, ϕ:

$$\Delta p(\phi) = \frac{2\sigma\cos\theta}{h} + \frac{2\sigma\cos(\theta+\phi)}{W - d\cos\phi}. \tag{2.3}$$

This is regarded as the cornerstone of bump-level analysis of the capillary flow. However, chip-level analysis is adopted instead to ease the formulation, by averaging the capillary pressure difference in (2.3) across the pitch:

$$\Delta\bar{p} = \frac{2\sigma\cos\theta}{h}\left(1 + \frac{h}{W}\int_0^{\frac{\pi}{2}} \frac{d\cos^2\phi}{W - d\cos\phi}\,\mathrm{d}\phi\right). \tag{2.4}$$

However, they used the averaged capillary pressure in (2.4) to compute the capillary force parameter that quantified the strength of capillary flow, as follows:

$$F = \frac{k_x \Delta\bar{p}}{\varepsilon}, \tag{2.5}$$

where k_x is the permeability along the flow direction, x and ε being the porosity. Qualitatively, F is higher when the gap height is smaller and bump pitch is larger, with the existence of critical pitch that gives $F = 0$. Young and Yang (2006) presented a generalized study on the effect of contact angle and solder bump arrangement on flip-chip underfill using the parameter F.

In the following year, Young (2003) refined the analysis of underfill flow by introducing the phenomenon of contact line jump (CLJ). This occurs when the meniscus just touches the solder bumps, where the contact line appears to jump forward instantaneously. It is assumed that the capillary pressure associated to this jump is large, so the reciprocal of capillary pressure in the integral is zero. Moreover, Young stated that the CLJ occurred at the values of ϕ between $-\pi/2$ and $-\pi/2 + \theta_b$

for quadrilateral bump array. However, the details on obtaining the position of occurrence of CLJ were not enclosed. This prompted Yao et al. (2014a) to criticize on Young's work on determining the amount of jumping is not based on any physics law. Subsequently, the flow velocity is derived based on the Darcy's law as in:

$$u(x_\mathrm{f}) = \frac{\mathrm{d}x_\mathrm{f}}{\mathrm{d}t} = -\frac{k_x}{\mu\varepsilon}\frac{\partial P}{\partial x_\mathrm{f}}. \tag{2.6}$$

The filling time, t_f is obtained by solving (2.6) with approximation of $\frac{\partial P}{\partial x_\mathrm{f}} \approx \Delta\bar{p}/x_\mathrm{f}$ to gives the second filling time model and subsequently referred as Young model.

Young (2004) developed another variant of filling time model by considering the viscous resistance and variable capillary pressure by the bump at different flow position. By integrating the pore velocity relation in equation (2.6) and by studying the mass conservation, one obtains:

$$\mu A^n(x_\mathrm{f})(R^{n+1} + \Delta R^n)\frac{\mathrm{d}x_\mathrm{f}}{\mathrm{d}t} = \Delta p. \tag{2.7}$$

$A^n(x_\mathrm{f})$ is the surface area of meniscus at position x_f while ΔR^n is the term due to viscous drag at n-th bump row. These parameters depend on whether the meniscus is located between bumps or after it passes the bumps, respectively given as:

$$A^n_{\mathrm{bump}}(x_\mathrm{f}) = (W - d\cos\phi)h\,, \tag{2.9}$$

$$\Delta R^n_{\mathrm{bump}} = \int_{-\pi/2}^{\phi} \frac{d\cos\phi}{2hk_x(W - d\,cos\phi)}\,\mathrm{d}\phi\,, \tag{2.10}$$

$$A^n_{\mathrm{afterbump}}(x_\mathrm{f}) = Wh\,, \tag{2.11}$$

$$\Delta R^n_{\mathrm{afterbump}} = \int_{-\pi/2}^{\pi/2} \frac{d\cos\phi}{2hk_x(W - d\,cos\phi)}\,\mathrm{d}\phi + \frac{12}{h^3W}(\Delta x^n_\mathrm{f} - d), \tag{2.12}$$

The filling time is obtained by solving for t_f in terms of x_f, from equation (2.7). This is regarded as the first and only filing time model that was based on bump-level

analysis, despite adopting the porous media assumption using Darcy's law. The imperfection of this model is on the constancy of effective permeability over one pitch, k_x, instead of varying based on a thin slab of meniscus flow. Moreover, the meniscus shape always assumed to be straight throughout the underfill flow. The CLJ introduced earlier in Young (2003) is not applied. Regardless of the downside, both ideas of segmentation in region and variables capillary pressure presented in this literature are the essences for developing a bump-level analysis-based filling time model.

Wan et al. (2005a) developed another analytical filling time model based on the simplified one-dimensional momentum equation for Couette flow, i.e. lubrication equation with additional power-law model of non-Newtonian fluid. This is the fourth filing time model and subsequently known as Wan model. Prior to the derivation of filling time model, Wan et al. (2005b) affirmed the influence of transient flow on the underfill process is negligible, thus the inertia term in momentum equation can be safely ignored. Wan model was based on chip-level analysis by averaging the driving capillary pressure over the chip but did not apply the porous media assumption and Darcy's law. By considering the solder bump as a square with side length of d, the resistance pressure exerted on the flow by the bump was derived through the principle of virtual work. The equation of Wan model is:

$$t_{\mathrm{f}} = \frac{2n+1}{n+1}\left[\frac{mhW(W+d)}{2\sigma\cos\theta\ (W^2+dW-dh)}\right]^{\frac{1}{n}}\left(\frac{2x_{\mathrm{f}}}{h}\right)^{\frac{n+1}{n}}, \tag{2.13}$$

where m and n are the constants associated to the power-law model. In fact, Wan model is the most popular analytical filling time model for validation study, since it is the most straightforward model available of reasonable accuracy. The major limitation of Wan model relies on the geometrical aspect of the flip-chip, which necessitate the term $W^2 + dW - dh$ to be larger than zero.

Subsequently, using the non-dimensionalized Wan model, Wan et al. (2007b) conducted a generalization study on the critical clearance at various gap height and flow behavior index, n. They found that there exists a threshold of bump pitch which will dramatically increase the filling time. Furthermore, the critical clearance increases with both the dimensionless gap height and n. Accordingly, a flip-chip package design protocol is formulated to ensure the bump clearance is less than the critical clearance.

After the successful consideration of non-Newtonian fluid viscosity in Wan model, Young (2010) proposed another model. Firstly, the experimental plot of viscosity against shear rate (Wang, 2007) is segmented into three segments of distinct trends. Later, the constitutive constants in each segments were determined. The momentum equation and power-law model by Wan et al. (2005a) is independently applied on these segmented. Later, the flow velocity is averaged over the gap-wise for all regions and lastly the filling time is obtained by using finite difference method.

Afterward, Young (2011) modified his permeability filling time model (Young, 2003) to predict non-Newtonian underfill flow. Both the viscosity, μ and permeability, k_x terms in equation (2.6) were replaced with the corresponding gap-wise averaged values. The Young power-law fluid filling time model was well-validated with his own simulation findings. It is also reported that the filling time increased steadily with n. Yang and Young (2013) computed the effective permeability of a three-dimensional unit cell of underfill flow in flip-chip for the use of analytical filling time model.

The fifth filling time model is analytically developed by Yao et al. (2014a) that is based on the permeability results from Yao et al. (2014b), and thereby known as Yao model. The governed equation of Yao model is Darcy's law, such that the flip-chip is assumed to be a porous media. Prior to determine the averaged driving pressure, both the meniscus evolution and CLJ as experimentally observed by Lee et al. (2010)

and Kim et al. (2012) were modelled analytically. Through conservation of mass with no-flow assumption, the jumping amounts at both entrance and exit CLJ were determined. Moreover, the capillary pressure is averaged temporally by weighing to the cross-sectional area of flow at each instant, for which the meniscus evolution and CLJ is incorporated at this stage. However, the Yao model was not pure analytical filling time model. The value of permeability, k is obtained from the correlation plots based on numerical simulation of unit-cell of flip-chip flow domain (Yao et al., 2014b). As Yao model is based on chip-level analysis, its final expression resembles the Washburn relation as follow:

$$t_{\mathrm{f}} = \frac{\mu\varepsilon}{2k\Delta\bar{p}} x_{\mathrm{f}}^{2}. \tag{2.14}$$

Upon comparing to other filling time models (Wan et al., 2005a; Young, 2003; Washburn, 1921), Yao model gave the closest filling time predictions to the experimental times.

The sixth filling model was presented by Luo et al. (2016). The Luo model is based on chip-level analysis and governed by the Darcy's law, though it differs in the formulations of effective permeability and averaged driving pressure. Like Wan model, the bump shape was assumed to be square and thus the flip-chip was reduced to a repetitive rectangular channel. The validation study showed that Luo model can predict the experimental filling times more accurate than the Wan model and Washburn model.

Yao et al. (2018) developed an analytical permeability model with accuracy comparable to their numerical permeability (Yao et al., 2014b). Later, Yao and Zhang (2018) improved their previous permeability model by additional consideration of the actual specific surface and tortuosity. Eventually, it is found that their latest permeability model gave even closer prediction to the numerical value. With these analytical permeability model, the revised Yao model is now purely analytical based.